Accepted Manuscript

Electrochemical performance of bulk-type all-solid-state batteries using small-sized $Li_7P_3S_{11}$ solid electrolyte prepared by liquid phase as the ionic conductor in the composite cathode

Marcela Calpa, Nataly Carolina Rosero-Navarro, Akira Miura, Kiyoharu Tadanaga

PII:	S0013-4686(18)32507-6
DOI:	10.1016/j.electacta.2018.11.035
Reference:	EA 33036
To appear in:	*Electrochimica Acta*
Received Date:	20 August 2018
Accepted Date:	06 November 2018

Please cite this article as: Marcela Calpa, Nataly Carolina Rosero-Navarro, Akira Miura, Kiyoharu Tadanaga, Electrochemical performance of bulk-type all-solid-state batteries using small-sized $Li_7P_3S_{11}$ solid electrolyte prepared by liquid phase as the ionic conductor in the composite cathode, *Electrochimica Acta* (2018), doi: 10.1016/j.electacta.2018.11.035

Graphical abstract

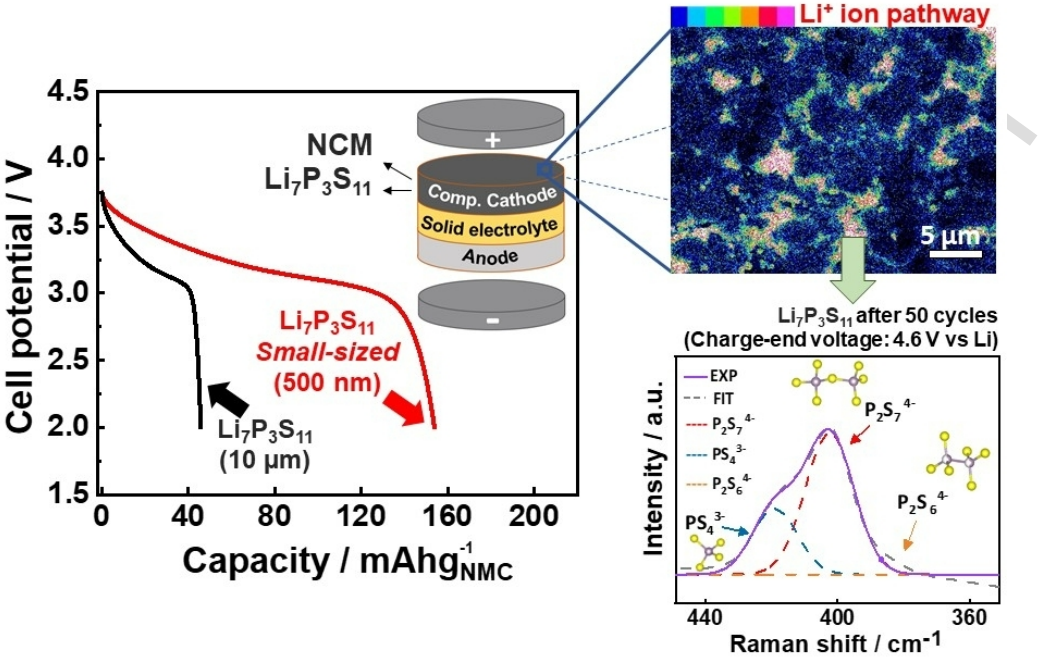

~~Application of $Li_7P_3S_{11}$ solid electrolyte prepared by liquid phase as ionic conductive additive in the composite cathode for bulk-type all-solid-state batteries~~

Electrochemical performance of bulk-type all-solid-state batteries using small-sized $Li_7P_3S_{11}$ solid electrolyte prepared by liquid phase as the ionic conductor in the composite cathode

Marcela Calpa[a], Nataly Carolina Rosero-Navarro[b*], Akira Miura[b] and Kiyoharu Tadanaga[b]

[a.] Graduate School of Chemical Sciences and Engineering, Hokkaido University, Sapporo 060-8628, Japan

[b.] Division of Applied Chemistry, Faculty of Engineering, Hokkaido University, Sapporo 060-8628, Japan

*E-mail address: rosero@eng.hokudai.ac.jp

Abstract

A high lithium-ion conductive solid electrolyte with $Li_7P_3S_{11}$ phase and small particle size was prepared by a liquid phase process, and the solid electrolyte was used as the ionic conductor in the composite cathode for bulk-type all-solid-state batteries. The electrochemical performance of the all-solid-state cell using $Li_7P_3S_{11}$ solid electrolyte prepared by liquid phase was studied and compared to that using $Li_7P_3S_{11}$ solid electrolyte prepared by ball milling.

Solid electrolytes prepared by the liquid phase and ball milling processes consisted mainly of the $Li_7P_3S_{11}$ crystal phase and the local structure was composed by PS_4^{3-}, $P_2S_7^{4-}$ and $P_2S_6^{4-}$ units. Both solid electrolytes exhibited a comparable high ionic conductivity over 10^{-3} Scm^{-1}. A particle size around 500 nm was obtained by the liquid phase process, while a particle size larger than 10 μm was obtained by the ball milling process. The composite cathode using the solid electrolyte obtained by the liquid phase process displayed a better distribution of the solid electrolyte and the active material, verified by scanning electron microscopy and energy-dispersive X-ray spectroscopy.

The all-solid-state cell using $LiNi_{1/3}Co_{1/3}Mn_{1/3}O_2$ and the solid electrolyte prepared by the liquid phase exhibited a better electrochemical performance than that using the solid electrolyte prepared by ball milling. The all-solid-state cells exhibited a first discharge capacity of 154 mAh g^{-1} and 46 mAh g^{-1}, respectively. Furthermore, the structure of the solid electrolyte prepared by the liquid phase process, after charge-discharge measurements with charge-end voltages of 4.6 V vs Li, was investigated by using ex-situ Raman spectroscopy. Significant structural changes were not observed, indicating that $Li_7P_3S_{11}$ is stable against charge-discharge processes.

Introduction

Development of good energy storage systems is essential to enable the use of renewable energy and electric vehicles[1, 2]. Li-ion batteries are promising candidates as they offer the high energy density that is required. However, conventional Li-ion batteries possess safety issue concerns due to the use of flammable organic liquid electrolytes. All-solid-state lithium batteries that use inorganic solid electrolytes instead of liquid electrolytes are expected to meet the required energy density and safety needs[3].

Sulfide-based solid electrolytes such as $Li_{10}GeP_2S_{12}$[4] and $Li_7P_3S_{11}$[5] exhibit high ionic conductivity comparable to liquid electrolytes, and have good deformability due to their low Young's modulus[6]. However, development of a favorable electrode-electrolyte interface in bulk-type all-solid-state batteries is still a challenge[7]. Bulk-type all-solid-state batteries use composite electrodes with a powder mixture of active materials and additives to improve both the electronic and lithium ion conduction[8]. Addition of carbon materials, such as VGCF (Vapor-grown carbon fiber), in a content of around 2 wt% is enough to achieve sufficient electronic conduction in the composite cathode[9]. However, a rather high content of solid electrolyte (60 wt%) is necessary to provide a good enough lithium ion conduction path[8]. A large interfacial contact area between active material and electrolyte particles and efficient ion-conductive pathways are necessary to obtain a good electrochemical performance in the all-solid-state battery[7, 10].

Solid electrolyte coating on active materials by using Pulser Laser Deposition (PLD) has been proven to be effective to obtaining high capacity and good electrochemical performance in the all-solid-state-cells, due to the formation of intimate electrode-

electrolyte contacts[11]. However, a scale-up of the PLD technique for commercial application may not be practical. A new approach is the use of small-sized solid electrolyte particles. It has been reported that dense and homogeneous electrode layers with an effective lithium-ion conduction pathway and a large electrode–electrolyte interfacial contact area can be formed by the use of smaller-sized solid electrolyte particles[12]. Sulfide solid electrolytes that are typically prepared by the ball milling process, are subsequently pulverized by using smaller diameter balls[12]. However, synthesis and pulverization, carried out by the ball milling process requires high energy and a long time.

Recently, we found that $Li_7P_3S_{11}$ solid electrolyte with high ionic conductivity (1×10^{-3} Scm^{-1} at 22°C) and small particle size can be synthesized by an instantaneous procedure involving a liquid phase process under ultrasonication and low heat treatment at 220 °C[13, 14]. The interaction between solvent and particles during the ultrasonication and the solvent removal led to obtaining the small particle size of around 500 nm. In contrast, sulfide solid electrolytes prepared by ball milling have particle sizes greater than 10 μm[12]. Moreover, the liquid phase process is a low energy synthesis, hence a more suitable process for a sustainable society.

On the other hand, it was found that the $Li_7P_3S_{11}$ solid electrolyte prepared by liquid phase possesses a wide electrochemical window up to 5 V (vs. Li/Li+)[14]. A wide electrochemical window enables the use of high voltage cathodes, which is important to achieve a high energy density. A solid electrolyte with high ionic conductivity, small particle size and wide electrochemical window is a suitable electrolyte to obtain a good ionic conduction path, a large electrode–electrolyte interfacial contact area in the composite cathode and high energy density in the all-solid-state battery by the use of high voltage cathodes.

In this study, we investigated the electrochemical performance of the all-solid-state battery using NCM ($LiNbO_3$-coated $LiNi_{1/3}Co_{1/3}Mn_{1/3}O_2$) as a high voltage cathode material[15], VGCF as an electronic conductive additive, favorable to form continuous electron conducting path within the electrode[8] and the $Li_7P_3S_{11}$ solid electrolyte, prepared by liquid phase, as the ionic conductor in the composite cathode, and compared it to that of the all-solid-state battery using $Li_7P_3S_{11}$ solid electrolyte prepared by ball milling as the ionic conductor in the composite cathode.

Experimental

In all experiments, samples were treated under an Ar atmosphere to avoid contact with the ambient atmosphere.

$Li_7P_3S_{11}$ powder was prepared by a liquid phase process[14]. Li_2S (Mitsuwa Chemical, 99.9%) and P_2S_5 (Aldrich, 99%) as starting materials were mixed in anhydrous acetonitrile (Wako Pure Chemical Industries). The mixture was ultrasonicated at 60 °C for 30 min under 28 kHz using an ultrasonic bath (Shimadzu SUS-103). The obtained slurry was dried at 180 °C for 3 h under vacuum to remove the solvent, and subsequently, the powder was heat-treated at 220 °C for 1 h.

$Li_7P_3S_{11}$ was synthesized by a ball milling process following a report by Tatsumisago et al.[6]. Mixture of Li_2S (Mitsuwa Chemical, 99.9%) and P_2S_5 (Aldrich, 99%) as starting materials was put into a zirconia pot (volume = 45 mL) with 500 zirconia balls (4 mm diameter). The mixture was ball-milled at 510 rpm for 10 h using a high-energy planetary ball mill apparatus. Subsequently, the resulting powder was heat-treated at 220 °C for 1 h, corresponding to the same heating temperature for the solid electrolyte prepared by liquid phase, to achieve similar ionic conductivity.

X-ray diffraction (XRD) patterns were measured by an X-ray diffractometer (Rigaku: Miniflex 600). Diffraction data was collected in 0.01° steps from 10° to 40° in 2θ.

Raman spectra were measured using a Raman spectrometer (HORIBA XploRA PLUS Scientific) to identify structural units of the solid electrolytes samples. The excitation and intensity of the laser beam were 532 nm and 17 mW, respectively.

Morphology of the sulfide solid electrolyte particles was observed by scanning electron microscopy (SEM), performed on a JIB-4600F Multibeam SEM-FIB Scanning Electron Microscope, with a sample transfer vessel system, where samples were not exposed to the ambient atmosphere.

The ionic conductivity of the pelletized samples was evaluated by the electrochemical impedance spectroscopy (EIS), under Ar atmosphere. The solid electrolyte powders (80 mg) were pressed under 360 MPa (at room temperature) in a polycarbonate tube with 10 mm of diameter, two stainless steel (SS) disks were used as current collectors. EIS measurements were conducted using an impedance analyzer (SI 1260, Solartron) in the frequency range of 1 MHz to 1 Hz at the amplitude of 30 mV.

Bulk-type all-solid-state cells were constructed as follows. $LiNbO_3$-coated $LiNi_{1/3}Co_{1/3}Mn_{1/3}O_2$ (NCM)[12, 16], $Li_7P_3S_{11}$ solid electrolyte and Vapor Grown Carbon Fiber (VGCF, Showa Denko), with a weight ratio of 79:19:2 were mixed to prepare the positive composite electrode. $80Li_2S{\cdot}20P_2S_5$ (mol%) glass and In metal (99.99% 0.1 mm thickness) were used as separator layer and anode, respectively. The $80Li_2S{\cdot}20P_2S_5$ (mol%) solid electrolyte was prepared by the ball milling process. A mixture of Li_2S and P_2S_5 was put into a zirconia pot (volume = 45 mL) with 500 zirconia balls (4 mm diameter) and was ball-milled at 510 rpm for 10 h. Bilayer pellets (φ = 10 mm) consisting of the positive composite electrodes (10 mg) and $80Li_2S□20P_2S_5$ solid

electrolyte (80 mg) were obtained by pressing under 360 MPa at room temperature; indium foil (40 mg) was then attached to the bilayer pellets by pressing under 240 MPa. The pellets were pressed using two stainless-steel rods; the stainless-steel rods were used as current collectors for both the positive and negative electrodes. All of the processes were performed in an Ar-filled glove box.

Charge-discharge performance of the cells was evaluated under a constant current (CC) mode at room temperature, under Ar atmosphere, using a charge-discharge measuring device (580 battery type system, Scribner Associates).

Results and discussion

The structure and properties of the sulfide solid electrolytes prepared by the liquid phase and ball milling processes were studied by using X-ray diffraction, Raman spectroscopy, scanning electron microscopy and electrochemical impedance.

Figure 1a shows the XRD patterns of the synthesized sulfide solid electrolytes, prepared by liquid phase and ball milling. The main peaks corresponding to the $Li_7P_3S_{11}$ phase were observed in both samples. The peak at 2θ = 27° in the sample prepared by liquid phase could be assigned to the Li_2S phase.

Figures 1b and 1c show the deconvolution of the Raman spectra of the sulfide solid electrolytes prepared by the liquid phase and ball milling processes, respectively. Deconvolution of Raman spectra was performed by using a Gaussian–Lorentzian function. Both Raman spectra displays a wide band centered around 401 cm^{-1}. Deconvolutions shows that the wide bands were composed by three bands centered around 420 cm^{-1}, 401 cm^{-1} and 385 cm^{-1} attributed to PS_4^{3-}(orthothiophosphate), $P_2S_7^{4-}$ (pyro-thiophosphate) and $P_2S_6^{4-}$ (hypo-thiodiphosphate) units, respectively.

Figure 2a shows the morphology of the sulfide solid electrolyte prepared by liquid phase. Irregular particles with particle size around 500 nm were observed. The particle size and morphology can be attributed to the interaction between solvent and particles during ultrasonication and solvent removal. The particle disaggregation produced during the ultrasonication process and the surfactant function that acetonitrile plays during the solvent removal may have led to obtaining the small individual particles[14]. Figure 2b shows the morphology of the sulfide solid electrolyte prepared by ball milling. A particle size larger than 10 μm was observed.

Figure 3 shows the impedance spectra of the pelletized samples. Both samples exhibited only a capacitive tail at high frequencies, which is attributed to the contribution of the interface between the solid electrolyte and the blocking stainless steel electrodes. Each resistance was estimated by the value of *Z*' at the intercept with the real axis obtained by linear fitting. The total ionic conductivity at room temperature of $Li_7P_3S_{11}$ solid electrolyte obtained by liquid phase and ball milling, attained 1×10^{-3} Scm^{-1} and 1.9×10^{-3} Scm^{-1}, respectively.

The evaluation of the prepared solid electrolytes by XRD diffraction exposed the formation of $Li_7P_3S_{11}$ as the main crystal phase in both samples. Raman spectroscopy indicated that structural units of PS_4^{3-}, $P_2S_7^{4-}$ and $P_2S_6^{4-}$ are contained in the structure of the solid electrolytes prepared by both processes. From crystal structural analysis, $Li_7P_3S_{11}$ consist only of PS_4^{3-} and $P_2S_7^{4-}$ units[17]. However, it has been observed the presence of $P_2S_6^{4-}$ units in the local structure of solid electrolytes containing the $Li_7P_3S_{11}$ phase[18, 19]. Studies by using MAS-NMR (magic angle spinning-nuclear magnetic resonance) spectroscopy suggest that the P_xS_y units remain in the amorphous phase after the crystallization[19]. Thus, it is assumed that the $P_2S_6^{4-}$ structural unit contained in the solid electrolytes prepared in this study may also be in

the amorphous phase. Although a similar wide Raman band was observed in both samples, the deconvolution of the Raman bands elucidates a different distribution of the P_xS_y units. The major fraction corresponds to $P_2S_7^{4-}$ units when the solid electrolyte was prepared by the liquid phase process and PS_4^{3-} units when the solid electrolyte was prepared by the ball milling process. Differences in the local structure can be due to the different reaction and crystallization mechanisms that take place by the liquid phase and ball milling processes.

Evaluation of the morphology by SEM shows that the particle size obtained by the liquid phase process is more than 10 times smaller than that of the particle size obtained by the ball milling process. Even though there is a significant difference in particle size between both solid electrolytes, the ionic conductivity evaluated by EIS showed that both exhibited a comparable ionic conductivity over 10^{-3} S cm^{-1}. Sulfide solid electrolytes possess a Young's moduli of about 20 GPa[6], which is around 10 times lower than that of the oxides solid electrolytes (about 200 Gpa[20, 21]). The low Young's moduli enable a room temperature pressure sintering, and therefore, the resistance of pelletized sulfide solid electrolytes is not largely influenced by the particle size. The slightly higher ionic conductivity of the solid electrolyte prepared by ball milling may be due to the different distribution of P_xS_y units in the local structure.

Both solid electrolytes exhibited the $Li_7P_3S_{11}$ crystal phase attaining comparable high ionic conductivity over 10^{-3} S cm^{-1}, and a different morphology. High ionic conductivity and a favorable morphology is necessary to obtain an effective lithium-ion pathway in the composite cathode, and therefore a good electrochemical performance in the bulk-type all-solid-state batteries. Thus, we investigated the influence of both $Li_7P_3S_{11}$ solid electrolytes prepared by liquid phase and ball milling processes, as the ionic conductor in the composite cathode for bulk-type all-solid-state batteries.

Figure 4 shows SEM images and energy-dispersive X-ray spectroscopy (EDX) elemental mappings for oxygen (O), manganese (Mn), phosphorous (P) and sulfur (S) of cross-sections of the composite cathode layers prepared by a simple mixture of NCM as cathode material, VGCF as electronic conductive additive and $Li_7P_3S_{11}$ synthesized by the ball milling and liquid phase processes as ionic conductive additive. The EDX elemental mappings of O and Mn show the distribution of NCM and the EDX elemental mappings of P and S show the distribution of the solid electrolyte. SEM and EDX images of the composite cathode with $Li_7P_3S_{11}$ prepared by ball milling process (Figure 4a), show large agglomerations of NCM particles, and large aggregates of solid electrolyte, greater than 20 µm. The poor distribution of the solid electrolyte in the composite cathode was expected due to its large particle size (Figure 2b). To obtain a good dispersion of solid electrolyte with large particle size is difficult due to the rather high active material content in the composite cathode. The SEM image of the composite cathode with $Li_7P_3S_{11}$ prepared by liquid phase process (Figure 4a), does not allow the identification of the solid electrolyte in the composite cathode. However, EDX analysis shows that the solid electrolyte was located between the NCM particles. A better distribution of the solid electrolyte through the composite cathode was observed, which is attributed to the small particle size of the solid electrolyte.

Figure 5 shows the first charge-discharge curves and cycle performance of all-solid-state cells with composite cathode fabricated with NCM, VGCF and $Li_7P_3S_{11}$ prepared by liquid phase and ball milling processes. The measurements were conducted using a constant current (CC) mode at a current density of 0.13 mA cm^{-2} and cut-off voltages of 3.8 and 2 V. The all-solid-state cell constructed using $Li_7P_3S_{11}$ prepared by the ball milling process had an initial discharge capacity of 46 mAh g^{-1}. The inhomogeneous distribution of NCM and solid electrolyte in the composite cathode layer (figure 4a)

resulted in a poor interfacial contact area between active material and electrolyte particles, and therefore in limited lithium ion-conductive pathways, which led to a deficient use of the active material. In contrast, the all-solid-state cell constructed using $Li_7P_3S_{11}$ prepared by the liquid phase process, had an initial discharge capacity of 154 mAh g^{-1}, more than three times higher than that of the all-solid-state cell using $Li_7P_3S_{11}$ obtained by the ball milling process. These results show that the better distribution of the solid electrolyte in the composite cathode, due to the small particle size of the $Li_7P_3S_{11}$ prepared by the liquid phase process, was effective in achieving more favorable lithium ion pathways to the NCM particles, and therefore achieving a larger discharge capacity. The all-solid-state cell with the composite cathode containing $Li_7P_3S_{11}$, prepared by the liquid phase process, exhibited a capacity retention of 81% after 30 cycles, and a coulombic efficiency over 99% after the first 3 cycles. The all-solid-state cell with the composite cathode containing $Li_7P_3S_{11}$ prepared by the ball milling process, exhibited a capacity retention of 87% after 30 cycles, and a coulombic efficiency over 99% after the first 10 cycles.

Figure 6a and b shows the impedance profiles of the all-solid-state cells of Figure 5 before charging and after the 30th cycle in the charged state. Before charging, both impedance profiles consist of an incomplete semicircle, due to the lower resistance, at high frequency (1 MHz) and a capacitive tail at low frequency (>100KHz), corresponding to the total resistance (Bulk and grain boundary) of the $80Li_2S\square20P_2S_5$ solid electrolyte used as separator layer (ca. 120 Ω), and the electrode interfaces (composite cathode and indium anode), respectively. After 30 cycles, two additional semicircles are observed in the impedance profiles. The top frequencies of the semicircles are 1 kHz and 1 Hz. The resistance observed at the medium (1 kHz) and low frequency (1 Hz) regions have been attributed to the resistances in the positive

electrode layer and the negative electrode layer, respectively[22]. Fitting results of the impedance profiles (solid line in Figure 6a and b) using the equivalent circuit of Figure 6c are shown in Table 1. The resistance at the high frequency region exhibited a similar value to that of before the battery cycling (ca. 120 Ω), in both cells. The high frequency resistance is essentially independent of the battery cycling since it corresponds to the lithium transport in the solid electrolyte used as separator layer. At the low frequency region (1Hz), no remarkable difference is observed between both cells (ca. 47 Ω). These results corroborate that both cells are equal at the separator and negative electrode layers, and that the different electrochemical behavior can be assigned to differences at the electrode-electrolyte interface at the positive electrode layer. The resistances at the medium frequency were determined to be 67 Ω and 25 Ω for the composite cathodes containing $Li_7P_3S_{11}$ prepared by liquid phase and ball milling processes, respectively. The resistance in the positive electrode layer has been explained by two possible mechanisms: formation of a space-charge layer at the interfaces[23] and interfacial chemical reactions that involves elements mutual diffusion between the oxide cathode materials and sulfide electrolytes[22]. Oxide coatings on cathode materials has been found to suppress the interfacial resistance[24]. However, development of completely uniform coating layers without any gap is difficult[16]. Thus, formation of the high-resistance interfaces in the positive electrode can be expected. From these results, the capacity decay observed in both cells may be attributed to the formation of the high-resistance interfaces. The larger resistance corresponding to the positive electrode layer that was found in the all-solid-state cell with the composite cathode containing $Li_7P_3S_{11}$ prepared by liquid phase, could be related to the possible presence of remaining organic complexes in the solid

electrolyte due to the liquid phase synthesis[25], and the larger interfacial contact area between active material and electrolyte particles.

The electrochemical behavior of the all-solid-state cell with composite cathode containing $Li_7P_3S_{11}$ prepared by liquid phase was investigated under high-charge-end voltages. After the first 30 charge-discharge cycles (cut-off voltages of 3.8 and 2 V), the all-solid-state cell was charged and discharged with cut-off voltages of 3.9 and 2 V for 10 cycles and subsequently with cut-off voltages of 4 and 2 V for 10 cycles. All measurements were conducted using a constant current (CC) mode at a current density of 0.13 mA cm^{-2}. Figure 7a shows the 30th, 40th and 50th discharge curves, corresponding to measurements performed with charge-end voltages of 3.8, 3.9 and 4 V, respectively. Figure 7b shows the corresponding cycle performance. The coulombic efficiency maintained at a value of around 99% for all cycles. According to the coulombic efficiency, a continuous capacity decay was observed.

Figure 8 shows the impedance profiles measured after the 40th (cut-off voltage of 3.9V) and 50th (cut-off voltage of 4V) charges of the all-solid-state cell of Figure 7. The impedance profiles are similar to that obtained after the 30th charge (Figure 6a). Two semicircles are observed, and the frequencies at the top of the semicircles are 1 kHz and 1 Hz. The resistances observed at the medium (1 kHz) and low frequency (1 Hz) regions correspond to the resistance in the positive and negative electrode layers, respectively, as discussed above. Fitting results of the impedance profiles (solid line in Figure 8) using the equivalent circuit of Figure 6c are shown in Table 2. A clear increase in the resistance at the medium frequency was observed after charge-discharge measurements with charge-end voltages of 3.9 (4.5 V vs Li) and 4 V (4.6 V vs Li), attaining 145 Ω and 318 Ω, respectively. The higher interfacial resistance in the positive electrode layer could be explained by the possible degradation of the active

material and sulfide electrolytes, due to the applied high charge-end voltages. It has been observed that NCM cathode material can undergo lattice volume changes upon charge, and that most pronounced changes occur at high charge-end voltages above 4.4 V[26, 27]. It has also been observed that sulfide solid electrolytes can undergo decomposition at the interfaces, above 4.5 V during charging process, which would result in the formation of isolating layers[28].

To investigate the possible degradation of the $Li_7P_3S_{11}$ solid electrolyte, the local structure of the solid electrolyte was analyzed by using ex-situ Raman spectroscopy after the charge-discharge measurements with high charge-end voltages. Ex-situ Raman spectroscopy was obtained for the composite cathode layer after the 50th cycle corresponding to the last measurement with charge-end voltage of 4 V (4.6 V vs Li). Figure 9b shows the deconvolution of the measurements average (900 points), by using a Gaussian–Lorentzian function. Two main peaks centered at 405 cm^{-1} and 420 cm^{-1}, corresponding to $P_2S_7^{4-}$ and PS_4^{3-} units were observed. Although no peak corresponding to the $P_2S_6^{4-}$ units was adjusted by the deconvolution, a scarce presence of these units was observed in the experimental data. Figure 9a shows the deconvolution of the Raman spectra corresponding to the as-prepared composite cathode for comparison. It has been reported that $Li_7P_3S_{11}$ solid electrolyte can go through changes in its structure under some input energy[13, 29]. Under heating at temperatures as high as 250 °C, structural changes proceeds to the formation of $P_2S_6^{4-}$ units which conduces to low ionic conductivity[13]. However, in the present study no additional formation of $P_2S_6^{4-}$ units in the structure of the $Li_7P_3S_{11}$ solid electrolyte, was found after charge-discharge measurements with high charge-end voltages. These results suggest that the $Li_7P_3S_{11}$ solid electrolyte did not suffer a significant structural change and that no degradation of the ionic conductivity can be expected after the

charge-discharge processes, even at high charge-end voltages. Hence, the formation of high-resistance interfaces in the positive electrode layer may be attributed to volume changes of the NCM material due to the use of the high charge-end voltage.

Conclusions

$Li_7P_3S_{11}$ sulfide solid electrolyte was prepared by using liquid phase and ball milling processes. Both solid electrolytes exhibited the formation of $Li_7P_3S_{11}$ as the main phase, and local structure composed by PS_4^{3-}, $P_2S_7^{4-}$ and $P_2S_6^{4-}$ units. A particle size around 500 nm and 10 μm was obtained by the liquid phase and ball milling processes, respectively. Both solid electrolytes presented a comparable ionic conductivity over 10^{-3} Scm^{-1}.

The application of the prepared solid electrolytes as the ionic conductor in the composite cathode of all-solid-state batteries was investigated. It was found that the particle size of the solid electrolyte largely influences the morphology of the composite cathode electrode. A non-homogenous distribution of solid electrolyte and active material particles was found in the composite cathode by using the solid electrolyte prepared by the ball milling process, due to the large particle size. In contrast, the small particle size of the solid electrolyte prepared by the liquid phase process enabled a better distribution of the solid electrolyte between the active material particles.

The all-solid-state cells using the NCM cathode material and the $Li_7P_3S_{11}$ sulfide solid electrolyte prepared by the liquid phase and ball milling processes, exhibited a first discharge capacity of 154 mA h g^{-1} and 46 mA h g^{-1}, respectively. This suggests that the use of small-sized solid electrolytes is effective to obtain favorable lithium ion

pathways in the composite cathode electrode, and therefore to achieve a better electrochemical performance in the all-solid-state battery.

The structure of the $Li_7P_3S_{11}$ solid electrolyte, prepared by liquid phase, in the composite cathode after charge-discharge measurements was investigated by using ex-situ Raman spectroscopy. Although, $Li_7P_3S_{11}$ can undergo structural changes, which proceeds to the formation of $P_2S_6^{4-}$ units, with some energy input, formation of $P_2S_6^{4-}$ units was not found after charge-discharge measurements with high charge-end voltages. This indicates that $Li_7P_3S_{11}$ is stable against charge-discharge measurements.

Acknowledgements

The present work was supported by the Japan Science and Technology Agency (JST), Advanced Low Carbon Technology Research and Development Program (ALCA), and Specially Promoted Research for Innovative Next Generation Batteries (SPRING) project. The analysis of SEM was carried out with JIB4600F at the “Joint-use Facilities: Laboratory of Nano-Micro Material Analysis”, Hokkaido University, supported by “Material Analysis and Structure Analysis Open Unit (MASAOU)”.

References

[1] B. Dunn, H. Kamath, J.M. Tarascon, Electrical Energy Storage for the Grid: A Battery of Choices, Science, 334 (2011) 928-935.

[2] D. Larcher, J.M. Tarascon, Towards greener and more sustainable batteries for electrical energy storage, Nature Chemistry, 7 (2015) 19-29.

[3] Y. Kato, S. Hori, T. Saito, K. Suzuki, M. Hirayama, A. Mitsui, M. Yonemura, H. Iba, R. Kanno, High-power all-solid-state batteries using sulfide superionic conductors, Nat. Energy, 1 (2016) 7.

[4] N. Kamaya, K. Homma, Y. Yamakawa, M. Hirayama, R. Kanno, M. Yonemura, T. Kamiyama, Y. Kato, S. Hama, K. Kawamoto, A. Mitsui, A lithium superionic conductor, Nat. Mater., 10 (2011) 682-686.

[5] Y. Seino, T. Ota, K. Takada, A. Hayashi, M. Tatsumisago, A sulphide lithium super ion conductor is superior to liquid ion conductors for use in rechargeable batteries, Energy Environ. Sci., 7 (2014) 627-631.

[6] A. Sakuda, A. Hayashi, M. Tatsumisago, Sulfide Solid Electrolyte with Favorable Mechanical Property for All-Solid-State Lithium Battery, Sci. Rep., 3 (2013) 5.

[7] A. Sakuda, A. Hayashi, M. Tatsumisago, Recent progress on interface formation in all-solid-state batteries, Curr. Opin. Electrochem., 6 (2017) 108-114.

[8] F. Mizuno, A. Hayashi, K. Tadanaga, M. Tatsumisago, Design of composite positive electrode in all-solid-state secondary batteries with Li2S-P2S5 glass–ceramic electrolytes, Journal of power sources, 146 (2005) 711-714.

[9] M. Tatsumisago, F. Mizuno, A. Hayashi, All-solid-state lithium secondary batteries using sulfide-based glass–ceramic electrolytes, Journal of power sources, 159 (2006) 193-199.

[10] A. Hayashi, A. Sakuda, M. Tatsumisago, Development of Sulfide Solid Electrolytes and Interface Formation Processes for Bulk-Type All-Solid-State Li and Na Batteries, Front. Energy Res., 4 (2016) 13.

[11] Y. Ito, M. Otoyama, A. Hayashi, T. Ohtomo, M. Tatsumisago, Electrochemical and structural evaluation for bulk-type all-solid-state batteries using Li4GeS4-Li3PS4 electrolyte coating on LiCoO2 particles, Journal of Power Sources, 360 (2017) 328-335.

[12] A. Sakuda, T. Takeuchi, H. Kobayashi, Electrode morphology in all-solid-state lithium secondary batteries consisting of LiNi1/3Co1/3Mn1/3O2 and Li2S-P2S5 solid electrolytes, Solid State Ionics, 285 (2016) 112-117.

[13] M. Calpa, N.C. Rosero-Navarro, A. Miura, K. Tadanaga, Preparation of sulfide solid electrolytes in the Li2S-P2S5 system by a liquid phase process, Inorganic Chemistry Frontiers, 5 (2018) 501-508.

[14] M. Calpa, N.C. Rosero-Navarro, A. Miura, K. Tadanaga, Instantaneous preparation of high lithium-ion conducting sulfide solid electrolyte Li7P3S11 by a liquid phase process, Rsc Advances, 7 (2017) 46499-46504.

[15] H. Kitaura, A. Hayashi, K. Tadanaga, M. Tatsumisago, Electrochemical performance of all-solid-state lithium secondary batteries with Li–Ni–Co–Mn oxide positive electrodes, Electrochimica Acta, 55 (2010) 8821-8828.

[16] N. Ohta, K. Takada, I. Sakaguchi, L.Q. Zhang, R.Z. Ma, K. Fukuda, M. Osada, T. Sasaki, $LiNbO_3$-coated $LiCoO_2$ as cathode material for all solid-state lithium secondary batteries, Electrochem. Commun., 9 (2007) 1486-1490.

[17] H. Yamane, M. Shibata, Y. Shimane, T. Junke, Y. Seino, S. Adams, K. Minami, A. Hayashi, M. Tatsumisago, Crystal structure of a superionic conductor, Li7P3S11, Solid State Ionics, 178 (2007) 1163-1167.

[18] M.R. Busche, D.A. Weber, Y. Schneider, C. Dietrich, S. Wenzel, T. Leichtweiss, D. Schroder, W.B. Zhang, H. Weigand, D. Walter, S.J. Sedlmaier, D. Houtarde, L.F.

Nazar, J. Janek, In Situ Monitoring of Fast Li-Ion Conductor Li7P3S11 Crystallization Inside a Hot-Press Setup, Chem. Mat., 28 (2016) 6152-6165.

[19] Y. Seino, M. Nakagawa, M. Senga, H. Higuchi, K. Takada, T. Sasaki, Analysis of the structure and degree of crystallisation of 70Li(2)S-30P(2)S(5) glass ceramic, Journal of Materials Chemistry A, 3 (2015) 2756-2761.

[20] Y.H. Cho, J. Wolfenstine, E. Rangasamy, H. Kim, H. Choe, J. Sakamoto, Mechanical properties of the solid Li-ion conducting electrolyte: Li0.33La0.57TiO3, J. Mater. Sci., 47 (2012) 5970-5977.

[21] G. Bucci, T. Swamy, Y.M. Chiang, W.C. Carter, Modeling of internal mechanical failure of all-solidstate batteries during electrochemical cycling, and implications for battery design, Journal of Materials Chemistry A, 5 (2017) 19422-19430.

[22] A. Sakuda, A. Hayashi, M. Tatsumisago, Intefacial Observation between LiCoO2 Electrode and Li2S-P2S5 Solid Electrolytes of All-Solid-State Lithium Secondary Batteries Using Transmission Electron Microscopy, Chem. Mat., 22 (2010) 949-956.

[23] K. Takada, N. Ohta, Y. Tateyama, Recent Progress in Interfacial Nanoarchitectonics in Solid-State Batteries, Journal of Inorganic and Organometallic Polymers and Materials, 25 (2015) 205-213.

[24] N. Ohta, K. Takada, L.Q. Zhang, R.Z. Ma, M. Osada, T. Sasaki, Enhancement of the high-rate capability of solid-state lithium batteries by nanoscale interfacial modification, Adv. Mater. (Weinheim, Ger.), 18 (2006) 2226-+.

[25] S. Chida, A. Miura, N.C. Rosero-Navarro, M. Higuchi, N.H.H. Phuc, H. Muto, A. Matsuda, K. Tadanaga, Liquid-phase synthesis of Li6PS5Br using ultrasonication and application to cathode composite electrodes in all-solid-state batteries, Ceramics International, 44 (2018) 742-746.

[26] A.O. Kondrakov, A. Schmidt, J. Xu, H. Gesswein, R. Monig, P. Hartmann, H. Sommer, T. Brezesinski, J. Janek, Anisotropic Lattice Strain and Mechanical Degradation of High- and Low-Nickel NCM Cathode Materials for Li-Ion Batteries, J. Phys. Chem. C, 121 (2017) 3286-3294.

[27] N. Yabuuchi, Y. Makimura, T. Ohzuku, Solid-state chemistry and electrochemistry of LiCo1/3Ni1/3Mn1/3O2 for advanced lithium-ion batteries III. Rechargeable capacity and cycleability, J. Electrochem. Soc., 154 (2007) A314-A321.

[28] G. Oh, M. Hirayama, O. Kwon, K. Suzuki, R. Kanno, Bulk-Type All Solid-State Batteries with 5 V Class LiNi0.5Mn1.5O4 Cathode and Li10GeP2S12 Solid Electrolyte, Chem. Mat., 28 (2016) 2634-2640.

[29] Y. Aoki, K. Ogawa, T. Nakagawa, Y. Hasegawa, Y. Sakiyama, T. Kojima, M. Tabuchi, Chemical and structural changes of 70Li(2)S-30P(2)S(5) solid electrolyte during heat treatment, Solid State Ionics, 310 (2017) 50-55.

FIGURES

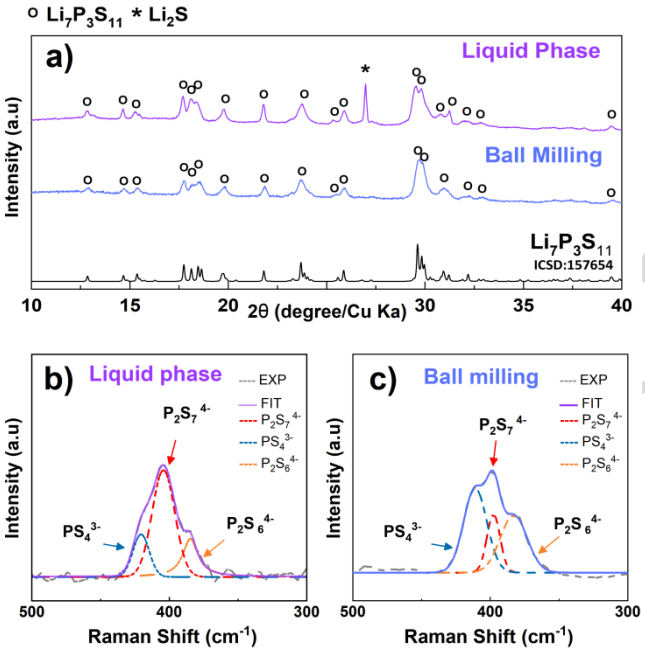

Figure 1. a) XRD patterns of the sulfide solid electrolytes prepared by liquid phase and ball milling. b) and c) Spectral deconvolution of Raman spectra of the sulfide solid electrolytes prepared by the liquid phase and ball milling processes, respectively. Spectra deconvolution was performed by using a Gaussian–Lorentzian function.

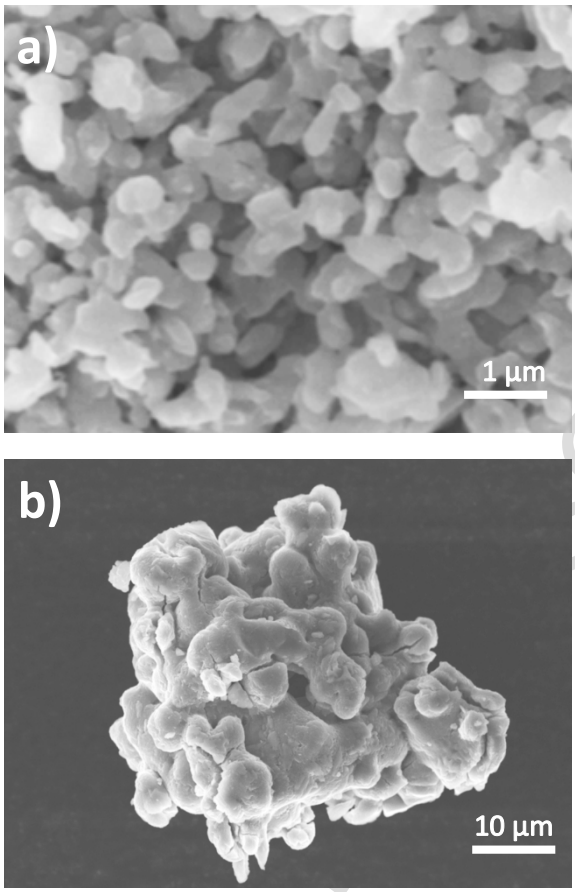

Figure 2. SEM micrographs of $Li_7P_3S_{11}$ prepared by the a) liquid phase and b) ball milling processes.

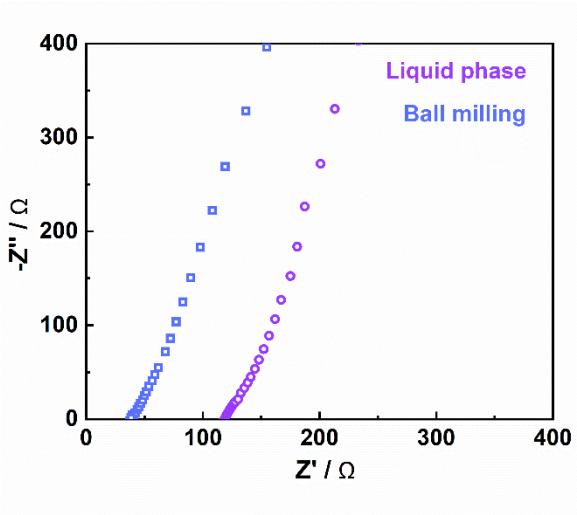

Figure 3. Impedance spectra of pelletized $Li_7P_3S_{11}$ solid electrolytes prepared by the liquid phase (purple circles) and ball milling (blue squares) processes.

Figure 4. SEM images and EDX elemental mappings for O, P, Mn and S of cross-section of the positive composite electrode layer using NCM as active material and $Li_7P_3S_{11}$ prepared by the a) ball milling and b) liquid phase processes as the ionic conductor.

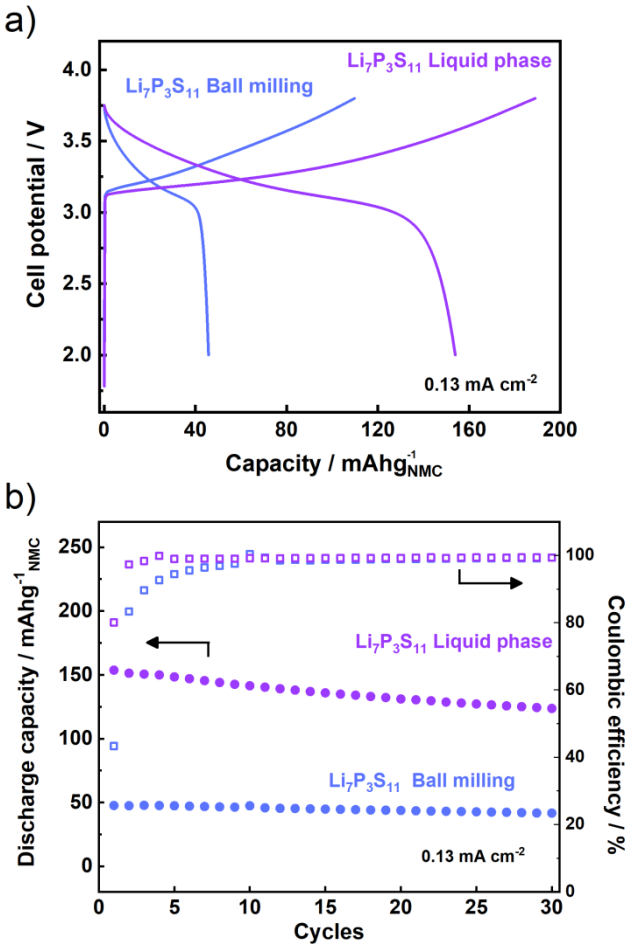

Figure 5. a) First charge-discharge curves and b) cycle performance of the all-solid-state cells using NCM as active material and $Li_7P_3S_{11}$ prepared by the liquid phase and ball milling processes as the ionic conductor in the composite cathode.

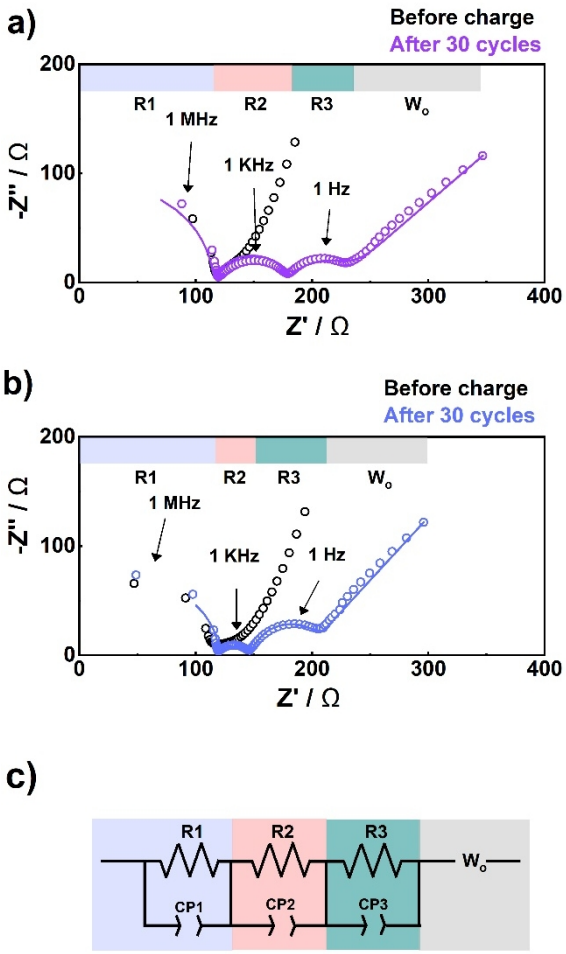

Figure 6. Nyquist plot of the impedance profiles of the all-solid-state cells using NCM as active material and $Li_7P_3S_{11}$ prepared by the a) liquid phase and b) ball milling processes as the ionic conductor in the composite cathode, before charge and after the 30th charge. Open circles represent the measured data, and solid lines indicated the fit of the data. c) Equivalent circuit for the impedance profiles fitting.

Table 1. Fitting Results of the EIS Spectra of the all-solid-state cells using NCM as active material and $Li_7P_3S_{11}$ prepared by the liquid phase and ball milling processes as ionic conductor in the composite cathode

Cell	R1	R2	R3
NCM/ $Li_7P_3S_{11}$ (liquid phase) before charge	119.6	-	-
NCM/ $Li_7P_3S_{11}$ (liquid phase) after 30 cycles	119.6	67	46
NCM $Li_7P_3S_{11}$ (ball milling) before charge	119.6	-	-
NCM/ $Li_7P_3S_{11}$ (ball milling) after 30 cycles	119.7	25	48

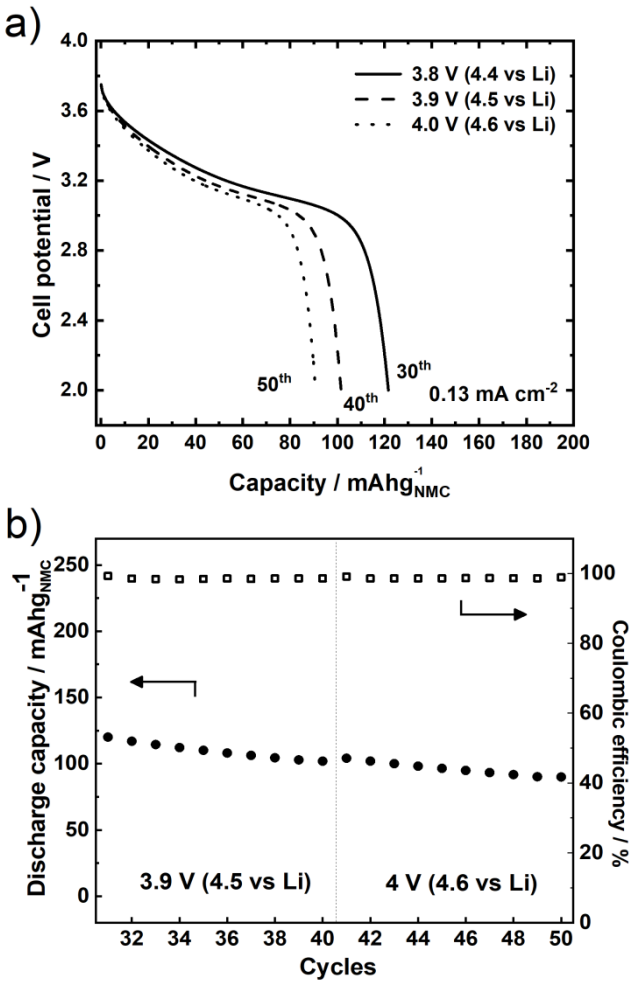

Figure 7. a) 30th, 40th and 50th discharge curves of the all-solid-state cell using NCM as active material and $Li_7P_3S_{11}$ prepared by the liquid phase process as the ionic conductor in the composite cathode, corresponding to measurements performed with charge-end voltages of 3.8, 3.9 and 4 V, respectively. b) Cycle performance corresponding to the charge-discharge measurements performed with charge-end voltages of 3.9 and 4 V.

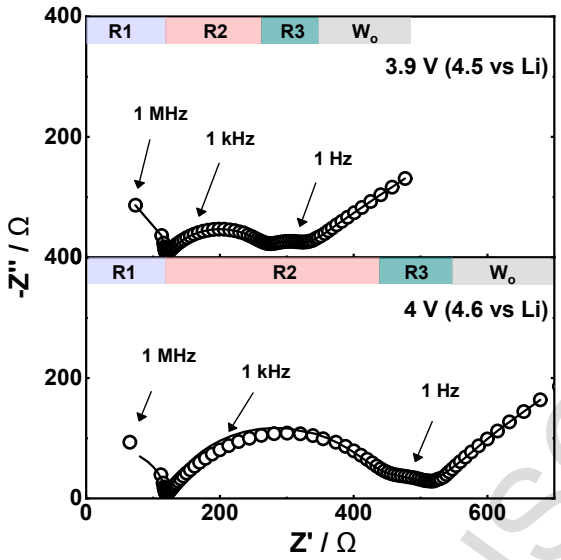

Figure 8. Nyquist plot of the impedance profiles of the all-solid-state cell using NCM as active material and $Li_7P_3S_{11}$ prepared by the liquid phase process as the ionic conductor in the composite cathode, after the 40th and 50th charge. Open circles represent the measured data, and solid lines indicated the fit of the data.

Table 2. **Fitting Results of the EIS Spectra of the all-solid-state cell using NCM as active material and $Li_7P_3S_{11}$ prepared by the liquid phase process as the ionic conductor in the composite cathode**

Charge-end voltage	R1	R2	R3
3.9 V	119.7	145	57
4 V	119.7	318	63

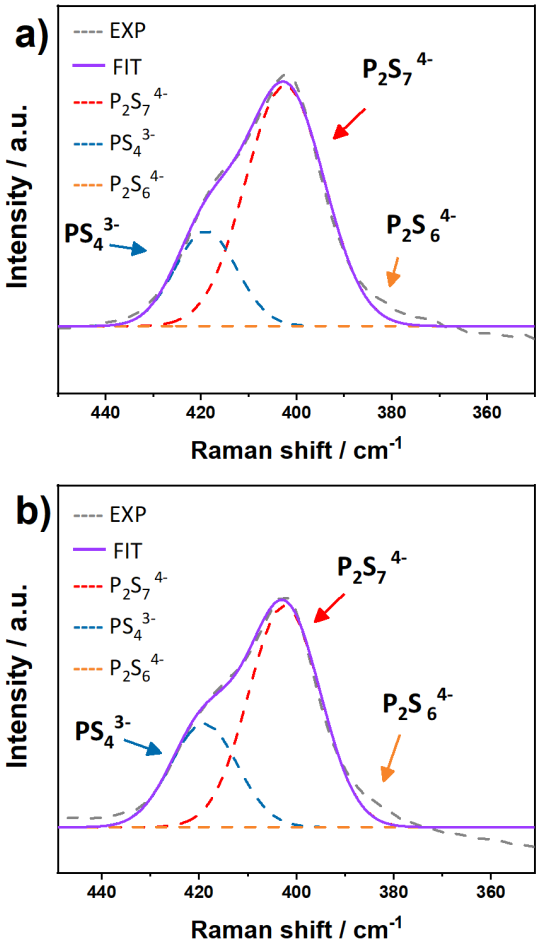

Figure 9. Spectral deconvolution of Raman spectra of a) the as-prepared composite cathode and b) the composite cathode layer after the 50th cycles (charge-end voltage of 4 V), by using a Gaussian–Lorentzian function.